2017-10-15

Classification of beach response to extreme storms

Burvingt, Olivier

10.1016/j.geomorph.2017.07.022
Geomorphology
Elsevier BV

Geomorphology 295 (2017) 722–737

Contents lists available at ScienceDirect

Geomorphology

journal homepage: www.elsevier.com/locate/geomorph

Classification of beach response to extreme storms

Olivier Burvingt *, Gerd Masselink, Paul Russell, Tim Scott

Coastal Processes Research Group, School of Biological and Marine Sciences, Plymouth University, Plymouth, UK

ARTICLE INFO

Article history:
Received 7 March 2017
Received in revised form 25 July 2017
Accepted 25 July 2017
Available online 04 August 2017

Keywords:
Storm response
Beach morphodynamics
Beach classification
LiDAR
Exposed beaches, sheltered beaches
Beach rotation

ABSTRACT

Extreme storms are responsible for rapid changes to coastlines worldwide. During the 2013/14 winter, the west coast of Europe experienced a sequence of large, storm-induced wave events, representing the most energetic period of waves in the last 60 years. The southwest coast of England underwent significant geomorphological change during that period, but exhibited a range of spatially variable and complex morphological responses, despite being subjected to the same storm sequence. Here, we use the 2013/14 storm response along the southwest coast of England as a natural field laboratory and explain this variability in storm response through the introduction and evaluation of a new classification of how sandy and gravel beaches respond to extreme storms. Cluster analysis was conducted using an unique data set of pre- and post-storm airborne Light Detection and Ranging (LiDAR) data from 157 beach sites based on the net volumetric change (dQ_{net}) and a novel parameter, the longshore variation index (*LVI*) which quantifies the alongshore morphological variability in beach response. Four main beach response types were identified: (1) fully exposed beaches that experienced large and alongshore uniform sediment losses ($dQ_{net} \approx 100\ m^3 \cdot m^{-1}$); (2) semi-exposed beaches that experienced medium alongshore uniform sediment losses ($dQ_{net} \approx 50\ m^3 \cdot m^{-1}$); (3) sheltered short beaches that experienced limited net sediment change and alongshore variability in beach response; and (4) sheltered long beaches that experienced considerable alongshore variability in beach response and large gross sediment change, but limited net sediment change. The key factors in determining the type of beach response are: exposure to the storm waves, angle of storm wave approach and the degree to which the beach is embayed. These factors are universally applicable on many exposed coastlines worldwide, so the response classification presented here is expected to be widely applicable.

1. Introduction

Within the next decades, coastal areas will have to face human and environmental challenges such as climate change, sea level rise and growing population (Jackson et al., 2013). While climate change and sea-level rise are gradual and global processes, coastlines are also affected by extreme and regional-scale events, such as extreme storms or sequence of storms.

The majority of storms that affect European Atlantic coasts originate in the mid-latitude westerly wind belt and are referred to as extratropical storms (Lozano et al., 2004). Storminess in the Atlantic due to extra-tropical storms is strongly linked to the North Atlantic Oscillation (NAO; Bromirski and Cayan, 2015) and the West Europe Pressure Anomaly (WEPA; Castelle et al., 2017), which are characterized by considerable inter-annual and inter-decadal variability. This temporal variability in atmospheric forcing is transferred to storminess and, in turn, to variations in the coastal response with short episodes of storm erosion alternated by longer periods of beach recovery (e.g., Scott et al., 2016). Coastal response to extreme storms is also characterized by significant spatial variability. Large-scale variability in storm response can generally be attributed to spatial variations in the hydrodynamic forcing (wave, tides and storm surge), but variability on a regional scale is more likely the result of site-specific conditions, such as beach type and/or local geology (Loureiro et al., 2012).

The extreme storm wave conditions in the Atlantic during the 2013/14 winter are considered the most energetic since at least 1948 (Masselink et al., 2016) and represent a recent example of the impact that large waves can have along the Atlantic coast of Europe. The wave conditions during this winter, specific to SW England, have been analysed by Masselink et al. (2015). They found that from October 2013 to April 2014, 22 storm-induced wave events, defined as events during which the peak significant wave height exceeded the 1% exceedance significant wave height, were recorded at the Seven Stones wave buoy 30 km off the tip of SW England. Wave conditions in these storms were outstanding, characterized by an average peak and mean significant wave height H_s of 8.1 m and 6.1 m, respectively, and peak wave periods of up to 22 s, and with an average storm duration of 29 h. On average, 17 storm events (peak $H_s > 4$ m) and 5 severe storm events

* Corresponding author at: Reynolds Building, Drake Circus, Plymouth, Devon PL4 8AA, UK.
E-mail address: olivier.burvingt@plymouth.ac.uk (O. Burvingt).

http://dx.doi.org/10.1016/j.geomorph.2017.07.022

(peak H_s > 6 m) occur annually (Scott, 2009). Two clusters of storms were associated with relatively large spring tides augmenting the storm surge (0.5–1 m), thus increasing storm wave impact at the coast. Most of the Atlantic coast of Europe, from Ireland to Portugal, was affected by these storms and their morphological impact on beaches has been well documented (Blaise et al., 2015; Castelle et al., 2015; Dissanayake et al., 2015; Masselink et al., 2015; Autret et al., 2016; Pye and Blott, 2016).

Beach response to extreme storms has been studied globally during the last decades and is naturally highly variable. Many factors account for this variability, including both the nature of the storm forcing and the characteristics of the coast (Cooper et al., 2004). Beach response to extreme storms is primarily dependent on the number of storms and their intensity. Recent studies showed that beach erosion resulting from a cluster of storms can be more extensive than an individual storm (Lee et al., 1998; Karunarathna et al., 2014; Senechal et al., 2015; Splinter et al., 2014a). However, erosion tends to reduce in magnitude and reach an equilibrium during an extended storm phase despite high energy levels being maintained (Aagaard et al., 2012). The chronological order of storms within a cluster in terms of intensity can also play a key role (Coco et al., 2014; Senechal et al., 2015). Storm wave height and peak wave period can be combined to calculate the storm wave power as a key parameter for relating wave forcing to morphological response (Splinter et al., 2014), and for defining a threshold for storm impact (Almeida et al., 2012). The tidal stage during the peak of the storm can also affect the coastal impact of the storm (Anthony, 2013; Masselink et al., 2015). Shoreline orientation relative to storm tracks will affect the wave incident angle and therefore influences beach and/or dune response through its control on longshore sediment transport (Costas et al., 2005; Anthony, 2013; Castelle et al., 2015). In addition to the sensitivity of coastal response to the forcing factors, variability in beach response is also affected by controlling factors such as beach morphology (Haerens et al., 2012), beach type (Qi et al., 2010) sediment size (Prodger et al., 2016) and geology (Loureiro et al., 2012).

Large-scale coastal change studies are relatively scarce (Barnard et al., 2015; Blaise et al., 2015; Masselink et al., 2016) and although better knowledge about beach response to extreme storms has been developed, many questions remain, such as the complex interplay between offshore wave characteristics, their transformation across the surf zone and pre-existing bathymetry (Coco et al., 2014). Moreover, studies about storm impact on beach response are often limited by the quantity of data and focus on a relatively small stretch of coastline or a small number of beaches (e.g., Lee et al., 1998; Costas et al., 2005; Qi et al., 2010; Aagaard et al., 2012; Almeida et al., 2012; Anthony, 2013; Coco et al., 2014; Karunarathna et al., 2014; Senechal et al., 2015; Splinter et al., 2014; Dissanayake et al., 2015; Castelle et al., 2015; Pye and Blott, 2016). The regional variability in the coastal response in SW England was of particular interest in recent studies (Masselink et al., 2015; Scott et al., 2016) where vastly different responses occurred to the same sequence of storms within SW England (Fig. 1).

The SW coast of England has a wide variety of beach types, geological boundaries and hydrodynamic conditions (Scott et al., 2011), and provides an ideal natural laboratory to investigate the factors that control the spatial variability in coastal response of a relatively large region to the same sequence of extreme storms. In their analysis of extreme storm response along the SW coast of England, Masselink et al. (2015) and Scott et al. (2016) mainly used morphological data derived from RTK-GPS cross-shore profiles surveyed at 38 beaches, and broadly distinguished between dominantly cross-shore and longshore beach responses. This paper extends this analysis by utilising vastly superior spatial coverage provided by airborne LiDAR surveys collected before

Fig. 1. Pictorial overview of storm impacts during the 2013/14 winter along the coast of SW England (numbers related to sites indicated in Fig. 2). (a) The gravel barrier at Westward Ho! #19 experienced overwash (photo: Richard Murgatroyd). (b1 before; b2 after) Large quantities of sand were removed from Whipsiderry beach #39, exposing the underlying rocky shore platform (photo: Mike Searle). (c) The seawall below Fistral Blu bar in Newquay #41 collapsed and causing damage to property (photo: Richard Murgatroyd). (d) The Watering Hole in Perranporth #46 required human interventions to protect the restaurant (photo from Mail Online, SWNS). (e) The coastal town of Looe #100 was flooded a number of times (photo: Nic Randall). (f) The coastal dunes at Thurlestone #119 experienced >5 m of erosion (photo: National Trust Southwest). (g) At the end of the winter, the beach in front of the seawall at Beesands #123 had completely disappeared. (h1 before; h2 after) The road that runs along the gravel barrier of Slapton Sands #124 became covered with gravel due to overwash (photo from BBC News, Press Association). (i) The most costly damage occurred to the London-Penzance railway line at Dawlish #139 (photo from BBC News, Press Association). This figure is available in colour online at https://www.journals.elsevier.com/geomorphology.

and after the 2013/14 winter on 157 beaches spread along the same coastline. The LiDAR data covers the entire intertidal beach area, enabling the response for each beach to be quantified in terms of a number of morphological change parameters, including net and gross volume change, and alongshore and vertical variability in the morphological response. A hierarchical clustering highlighted four key types of beach response, differentiated by the net intertidal beach volumetric change and longshore variability in beach response. Wave forcing proxies and geological variables were used to evaluate their role in causing the observed the regional variability in the coastal response.

2. Study area and datasets

2.1. Study area

Along the southwest coast of England, Devonian and Carboniferous slates, shales, sandstones and limestone were intensely deformed, and then intruded by highly resistant granite bodies (Clayton and Shamoon, 1998), producing a diverse coastal scenery. The area itself was not glaciated, but periglacial processes resulted in the production of large quantities of superficial sediments, occupying a full spectrum of sediment sizes from mud to boulders. This peninsula, which can be divided in north and south coast (Fig. 2), offers a large number of beaches, including long and wide sandy beaches, gravel barriers, small pocket beaches and beaches backed by extensive dunes systems or high rocky cliffs. The high diversity in beach morphology is due to variable dynamic (waves, tides) and static (shoreline orientation, geology, sediment size and abundance, bar morphology) boundary conditions, and has led to the identification of nine distinct beach types ranging from fully reflective to ultra-dissipative beaches (Scott et al., 2011). Beach type was found to be mainly controlled by the average wave/tide conditions and sediment size characteristics, but geological setting was also found to play a significant role.

For this study, 157 beaches are considered, numbered sequentially in an anti-clockwise direction, and the study sites are distributed fairly evenly along the SW coast of England. They are located in the following five regions (Fig. 2).

2.1.1. Somerset (#1–16)

The first 16 sites are located along the southern margin of the Bristol Channel in Somerset. Waves are predominantly incident from the west with 10% exceedance significant wave height, $H_{s10\%}$, ranging from 1 to 2 m and the tidal range is the largest in the region (mean spring tide range 8 to 12 m) (BERR, 2008). The coastal geomorphology is characterized by rapidly eroding cliffs (Minehead #7) and the eastward longshore drift has result in a full suite of accretionary landforms: sandy beaches (Weston-super-Mare #2), storm ridges (Porlock #10), salt marsh (Steart #4), and sand dunes (Berrow sand #3) (Kidson et al., 2008).

2.1.2. North Devon (#17–21)

Proceeding along the coastline in an anticlockwise direction, 5 study sites are located in North Devon. The sites facing west are very large sandy beaches backed by imposing dune systems (at Croyde #17 and Saunton #18) while the sites facing north are relatively small beaches constrained between rocky platforms (Bucks Mills #20 and Shipload Bay #21). This stretch of coastline experiences a smaller tidal range (mean spring tide range from 7 to 8 m) and larger wave exposure from the west ($H_{s10\%}$ between 2 and 3 m) than the study sites in Somerset (BERR, 2008).

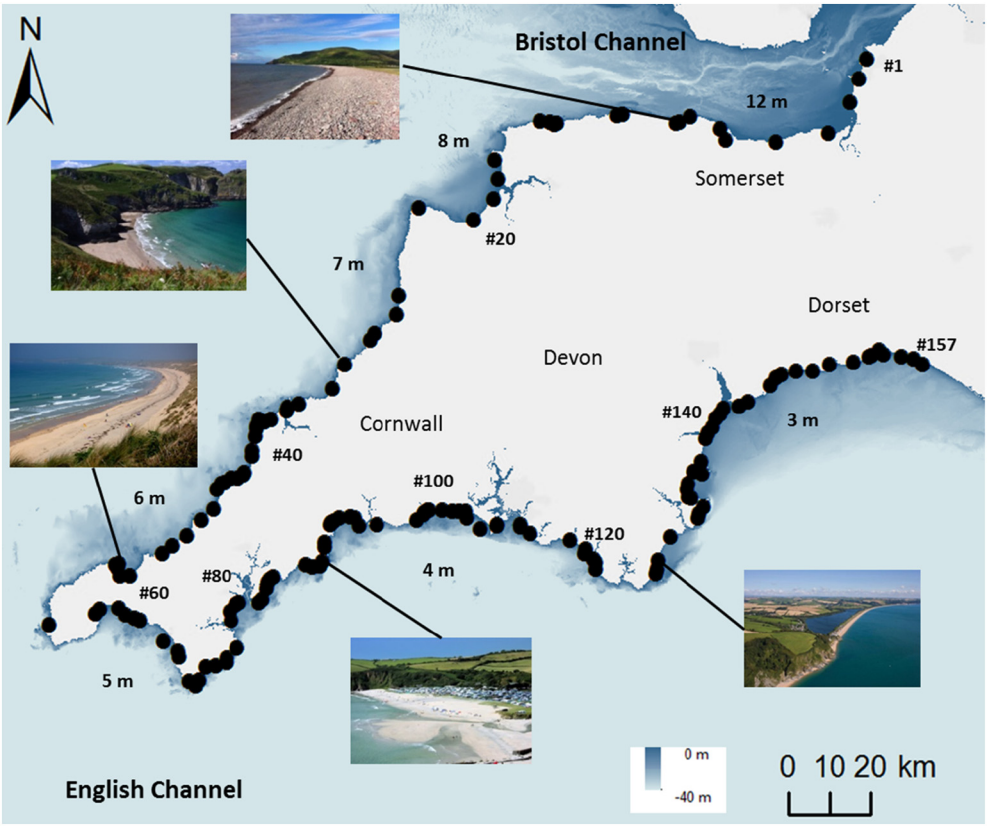

Fig. 2. Map of SW England and location of the 157 beaches for which LiDAR data are available. Pictures of (anti-clockwise): Porlock #10, Bossiney #26, Hayle #51, Pentewan #90 and Slapton Sands #124, illustrating the diversity of beach systems along the SW coastline of England. Black numbers indicates the different tidal ranges along the coast. This figure is available in colour online at https://www.journals.elsevier.com/geomorphology.

2.1.3. North Cornwall (#22–56)

The next 35 sites are located along the north coast of Cornwall which is characterized by sandy beaches with high cliffs (Bude #22), rocky headlands (Porthtowan #48) and several large coastal sand dune systems (Gwithian #51, Perran Sands #46). The mean spring tide range decreases from north (7 m) to south (5 m) with $H_{s10\%}$ ranging from 2 to 4 m (BERR, 2008).

2.1.4. South Cornwall (#57–113)

Cornering the tip of the peninsula, the 57 sites spread along this stretch of coastline are highly variable, but mainly consist of coarser sand beaches interspersed by rocky sections (Penzance #58 and Marazion #59 for example). Beaches are more sheltered from wave energy coming from the west compared to the north coast of Cornwall, but some are fully exposed to SW wave energy (and also potentially from SE wind waves). Wave exposure is highly dependent on the shoreline orientation -which varies greatly along this stretch of coast. The mean spring tide range and 10% exceedance significant wave height generally decreases from west to east (5 to 4 m and 4 to 2 m, respectively) (BERR, 2008).

2.1.5. South Devon (#114–157)

The last 44 study sites are located in South Devon and Dorset. Similar to the south coast of Cornwall, the study sites along the western part of this stretch of coast consist of coarse-sand beaches interspersed by rocky sections (Challaborough #117, Milton Sands #120). Further east, a large number of thin and long beaches composed of a mixture of sand and gravel can be found (Slapton Sands #124, Sidmouth #146, West Bay #157). Shoreline orientation is also very variable and largely determines wave exposure. The mean spring tide range and $H_{s10\%}$ generally decreases from west to east (4 to 3 m, 2 to 1 m, respectively) (BERR, 2008).

2.2. LiDAR dataset

Commissioned by the Environment Agency (EA), the coastline of SW England is surveyed every few years by airborne LiDAR (http://www.channelcoast.org/southwest/). Different sections of the coast are surveyed in different years, almost always during the spring months, and the whole coast was surveyed in spring 2014 following the extreme events of the winter 2013/2014. Airborne LiDAR surveys are usually carried out during spring tides to maximise beach coverage. Every beach in SW England with at least 70% LiDAR coverage is used for analysis, resulting in 157 study sites spread out along the SW peninsula with 56 beaches located on the north coast and 101 on the south coast (Fig. 2).

Airborne LiDAR data has the advantage of offering a large spatial coverage and can be used to produce digital elevation models (DEMs) with at least 1-m horizontal spatial resolution, but in comparison to in-situ survey methods, the vertical accuracy of LiDAR is lower. Whereas RTK-GPS measurements have c. ± 3 cm vertical accuracy (Harley et al., 2011), the vertical accuracy of LiDAR data is c. ± 15 cm (Sallenger et al., 2001). However, many studies showed that the accuracy of LiDAR surveys does not impede the quantification of large morphological changes due to extreme events and its extensive spatial coverage makes it a valuable tool to study beach morphological change (White and Wang, 2003; Saye et al., 2005; Sallenger et al., 2001; Sherman et al., 2013; Pye and Blott, 2016).

Since LiDAR campaigns have not been carried out every year at each site, the timing of the 'pre-storm' datasets is an issue. The most recent pre-storm surveys were carried out in April 2012, while the oldest pre-storm surveys dated from October 2010. Since this study focuses on the changes that occurred during the winter of 2013/14, for many beaches the pre- and post-storm datasets are >2 years apart. This makes attributing the difference in morphology to the 2013/14 storms potentially problematic. However, analysis of monthly survey data from Perranporth (North Cornwall) demonstrates that by far the most significant change in beach volume occurred during the 2013/2014 winter period along the north coast, and that the spring beach volumes during 2010, 2012 and 2013 were very similar (Masselink et al., 2016; Scott et al., 2016). Along the south coast, morphological changes observed at Slapton Sands (South Devon) observed during the 2012/13 winter were significant in comparison to the previous winters, but relatively small compare to the 2013/14 winter (Scott et al., 2016). In addition, annual surveys collated/conducted by the Plymouth Coastal Observatory also demonstrate the unprecedented nature of beach profile changes at many beaches in Cornwall and Devon in 2013/14 (http://www.coastalmonitoring.org/reports). The changes in beach volume derived from the LiDAR data are therefore considered to represent mainly the changes that occurred during the 2013/14 winter.

Preparing the LiDAR data for analysis comprises a number of processing steps, ultimately leading to the extraction of overlapping pre- and post-storm DEMs corresponding to the active area of the beach. Fig. 3 shows this process for two adjoining beaches located on the north coast of Cornwall (Fistral #42 and Crantock #43). LiDAR surveys generally extend from Spring Low Water Level to several 100 m landward and the beach area cannot be directly and easily identified (Fig. 3a). Therefore, using high resolution aerial pictures (Fig. 3b), every beach area was digitized by drawing polygonal shapefiles on ArcMap 10.2.2 software (Fig. 3c). The beach areas were digitized accurately and included the active beach/dune area based on tide and surge water levels, but excluded relatively static elements such as coastal cliffs, large rock outcrops and infrastructure. The beach area captured by these shape files did not extend beyond the spatial limitations of the LiDAR data. Then, using the same coordinate system (British National Grid Projected Coordinates System), both beach area shapefiles and LiDAR rasters were overlapped (Fig. 3d) and the overlapped data were extracted. The extraction is done twice (pre- and post-storm rasters, using same beach area shape file) for each of the 157 beaches, and the post- and pre-storm rasters are subtracted to obtain a difference DEM, also referred as DoD (Wheaton et al., 2010) (Fig. 3e). These DoDs are then converted into ASCII files, to be next processed with Matlab R2013®. A GoogleEarth dataset for the 157 DoDs is also available from the online article.

3. Methods

3.1. Beach response variables

The DoDs were used to extract a range of parameters that best quantify the morphological storm response. The most obvious of these are the net volumetric change, the gross volumetric change and the vertical change.

The total volumetric change dQ_{tot} (in m^3) corresponds to the difference in beach volume between the post- and pre-storm DEM and quantifies the total volume of sediment lost or gained over the survey period, attributed to the 2013/14 storm season:

$$dQ_{tot} = \sum_1^N dQ_i \quad (1)$$

To compare the total volumetric change between different study sites, dQ_{tot} is normalized by beach alongshore length L_S (in m), yielding the net volumetric change per unit m beach width, dQ_{net} (in $m^3 \cdot m^{-1}$ or m^2):

$$dQ_{net} = {}^1/_{L_S} \sum_1^N dQ_i \quad (2)$$

The gross volumetric change per unit meter beach width, dQ_{gross} (in $m^3 \cdot m^{-1}$ or m^2) corresponds to the sum of the absolute value of

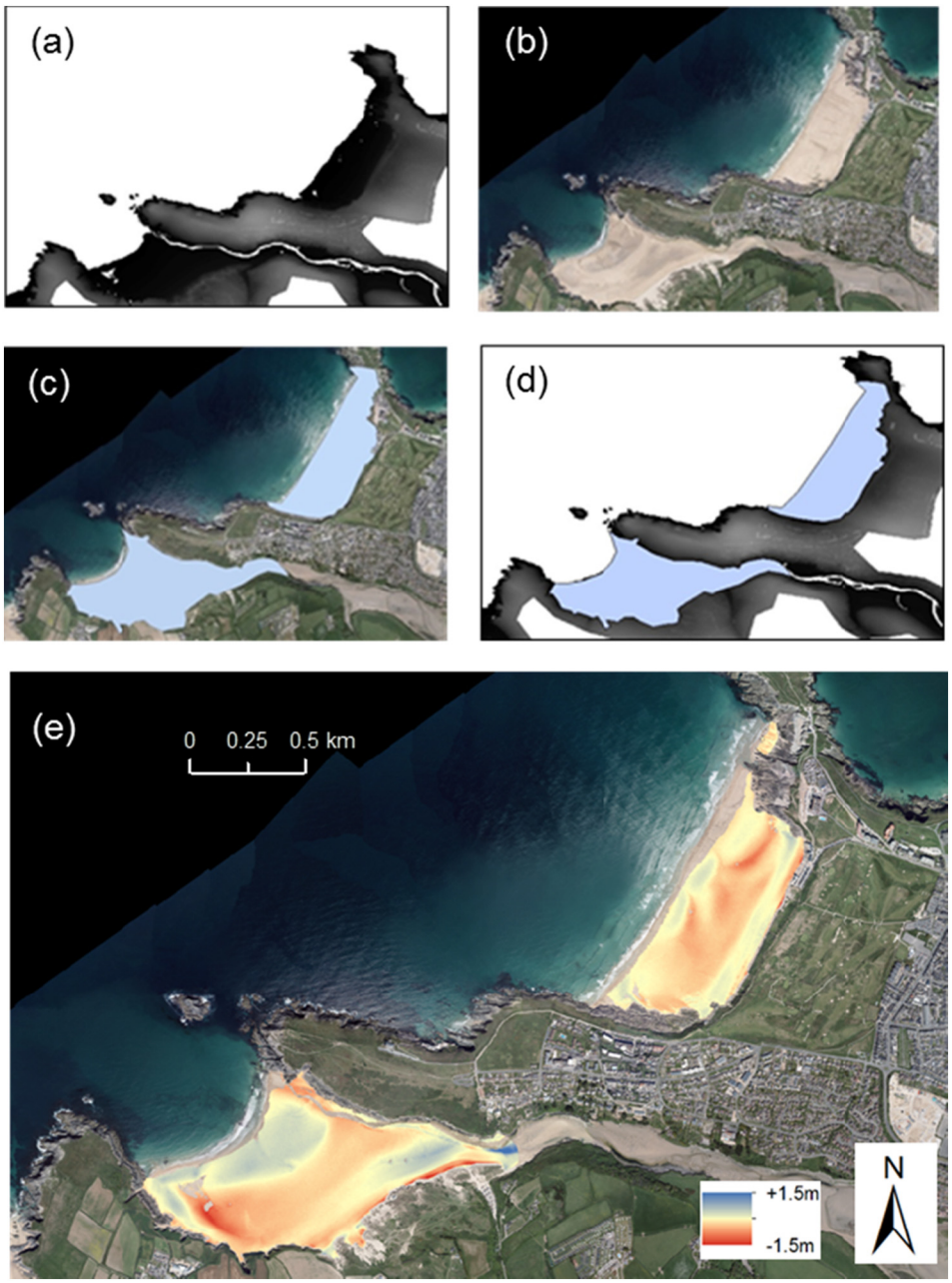

Fig. 3. Illustration of the process of extracting useful data from the LiDAR titles: (a) raw LiDAR data; (b) aerial picture of the same area; (c) digitized shapefiles drawn around the two beaches (Fistral #42 and Crantock #43); (d) digitized shapefiles overlapped with LiDAR data; and (e) the image of subtracted new rasters of LiDAR data surveyed in April 2012 (pre-storm) and April 2014 (post-storm) at both sites. This figure is available in colour online at https://www.journals.elsevier.com/geomorphology.

topographic change between post- and pre-storm DEM normalized by the length of the beach L_S (in m):

$$dQ_{gross} = {}^{1}/_{L_s} \sum_{1}^{N} | dQ_i | \quad (3)$$

This variable represents the total volume of sediment that has been mobile along the beach during the 2013/14 winter period. The mean vertical elevation change dz (in m) corresponds to the total volumetric change divided by the surface area of the active beach area S (in m^2):

$$dz = {}^{1}/_{S} \sum_{1}^{N} dQ_i \quad (4)$$

The net volumetric change per unit meter beach width for different areas of the beach was also calculated. The beach area was divided into three zones based on the tidal levels: (1) a lower beach area was defined as extending between the lowest level surveyed during LiDAR measurements (usually just above mean low water spring level MLWS), and mean sea level (MSL); (2) an upper area was defined between MSL and mean high water springs (MHWS); and (3) a supra-tidal area was defined between MHWS and the top of the active area of the beach/dune system. The volumetric changes corresponding to these three different areas (dQ_{lower}, dQ_{upper} and dQ_{dune}, respectively) were calculated using Eq. (2) using the appropriate tidal level.

All morphological change parameters defined above disregard the alongshore variability in the beach response and a parameter was formulated to quantify the alongshore morphological variability, which can be considerable (Fig. 4a). The DoD rasters are first rotated onto a local coordinate system, such that the cross-shore and alongshore direction of the beach represent the x- and y-coordinate, respectively

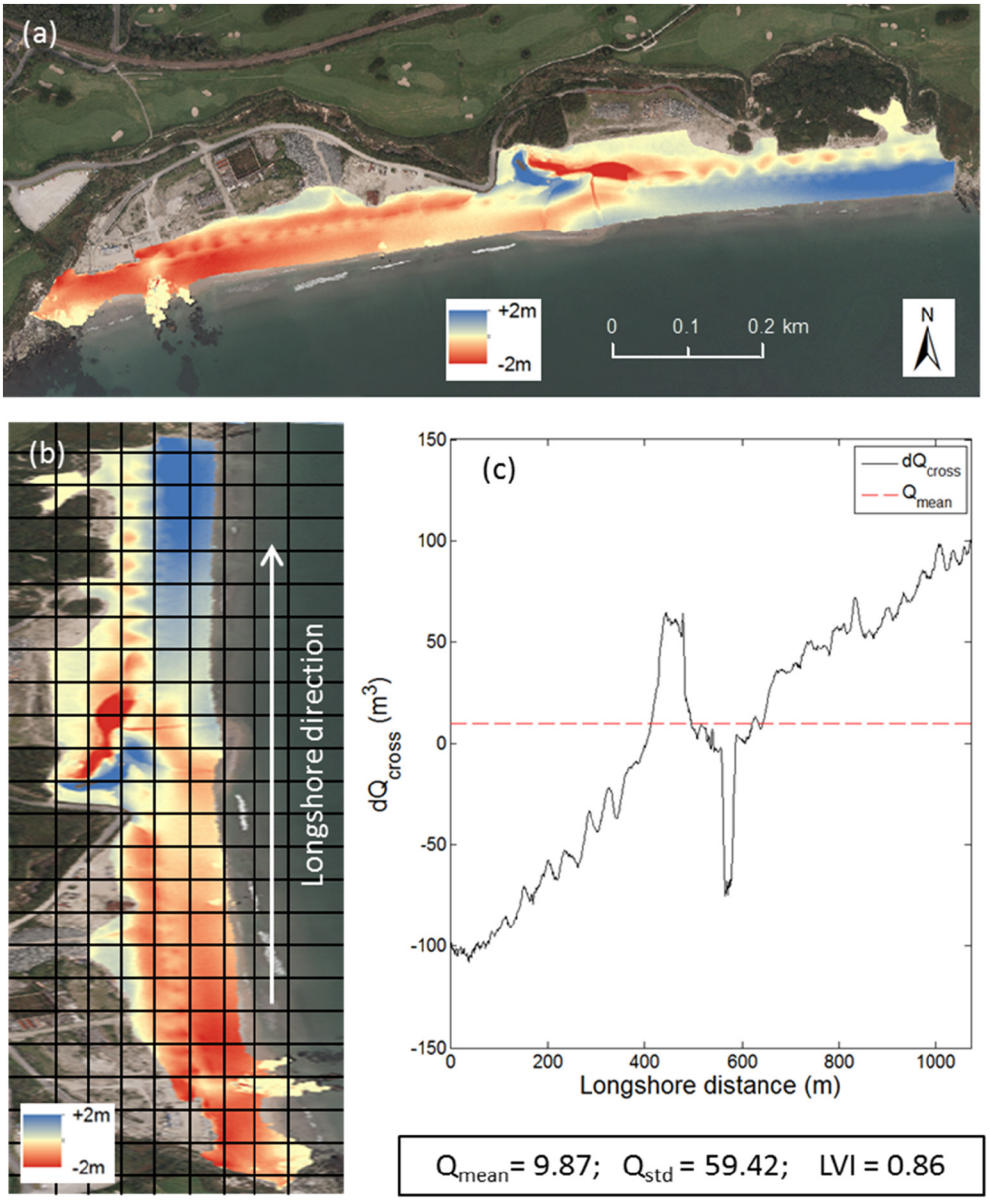

Fig. 4. Illustration of the process of calculating longshore variation index (*LVI*): (a) example of DoD obtained when post- and pre-storm LiDAR rasters are subtracted at Carlyon beach #94 (surveyed in May 2014 and March 2012, respectively); (b) rotated DoD overlapped with a grid in which every row of data represents a 1 m cross-shore transect and every column a 1 m longshore one (not to scale for graphic purpose); (c) alongshore variation in the net cross-shore volumetric change dQ_{cross} with the alongshore-averaged change Q_{mean} plotted as a horizontal red line and values of the variables used in Eq. (5). This figure is available in colour online at https://www.journals.elsevier.com/geomorphology. (For interpretation of the references to colour in this figure legend, the reader is referred to the web version of this article.)

(Fig. 4b). The grid size of this rotated raster remains 1 m and the net volumetric change dQ_{cross} is determined for each cross-shore transect, providing information on the alongshore variation in the cross-shore volumetric change (Fig. 4c). Then, the standard deviation Q_{std} is used to quantify the amount of variation of all the dQ_{cross} values. The longshore variation in the morphological response *LVI* is then defined as:

$$LVI = \frac{Q_{std}}{|Q_{mean}| + Q_{std}} \quad (5)$$

where $|Q_{mean}|$ is the absolute value of the mean of dQ_{cross} values and is used to normalize Q_{std} values between the different beaches. This index is dimensionless and varies between 0 and 1 with higher values representing greater longshore variability in beach response. The parameter is not simply representing the ratio between longshore and cross-shore sediment transport, $LVI = 1$ implied longshore sediment transport dominance, and $LVI = 0$ indicates cross-shore sediment transport is dominant, but a non-zero value for *LVI* can also be caused by an along-coast variation in cross-shore sediment transport.

3.2. Geological control

Geological boundaries can play an important role in beach dynamics (Jackson et al., 2005; Scott et al., 2011). To consider the impact of embayment dimensions and geometry on beach response, the dimensionless embayment scaling parameter is generally used (Short, 1999; Castelle and Coco, 2012; Loureiro et al., 2012). This parameter relates the embayment configuration to the incident breaking wave conditions. Here, due to the absence of inshore wave conditions data for every beach, the normalized beach length, *NBL*, was computed as the ratio

between the beach alongshore length L_s and the cross-shore length L_c (from MLWS to MHWS):

$$NBL = {}^{L_s}/_{L_c} \quad (6)$$

'Short' embayed beaches are characterized by small *NBL* values whereas for 'long' beaches, *NBL* approaches 1. This parameter remains valid for open beaches that do not exceed 6.5 km in the present study, the mean alongshore beach length for all study sites is equal to 1.3 km.

3.3. Offshore wave data and forcing

Modelled wave data were obtained from the Met Office's 8-km grid WAVEWATCH III model, one of the most frequently used model for wave simulation that has been validated for extreme events (Moon et al., 2003). 46 grid points located around the SW coast of England were selected for this study (Fig. 5). The water depths vary between 15 and 50 m dependent on the cell location, and grid points are considered to be in deep water. For each model grid point, hourly values of significant wave height H_s, wave energy period T_e, and wave direction were extracted for the 3-month period from 1 December 2013 to 28 February 2014, corresponding to 2160 h of data for each grid point. For comparative purposes, wave data were also obtained from the relatively clam 2012/13 winter.

Offshore wave power *P* was used to quantify wave forcing and was calculated for every hour using the deep water wave equation (Herbich, 2000):

$$P = \frac{1}{64\pi}\rho g^2 {H_s}^2 T_e \quad (7)$$

where ρ is water density and g is gravity. The offshore wave power *P* calculated at each grid point was averaged over the 3-month winter period and Fig. 5a shows the distribution of the 2013/14 winter average wave power value $|P|$ along the SW of England. Generally, the north coast received more wave power than the south coast because it is more exposed to the prevailing waves approaching from the west. Along the north coast, $|P|$ increases from 20 kW m^{-1} to 100 kW·m^{-1} at the tip of the peninsula. Along the south coast, $|P|$ decreases in an eastward direction from 90 to 10 kW·m^{-1}.

Recent beach response models (e.g. Davidson et al., 2013; Castelle et al., 2014; Splinter et al., 2014b; Scott et al., 2016) have highlighted that wave conditions relative to the long-term antecedent wave conditions, referred to as disequilibrium wave conditions, are more important in driving beach change than the instantaneous wave conditions. Based

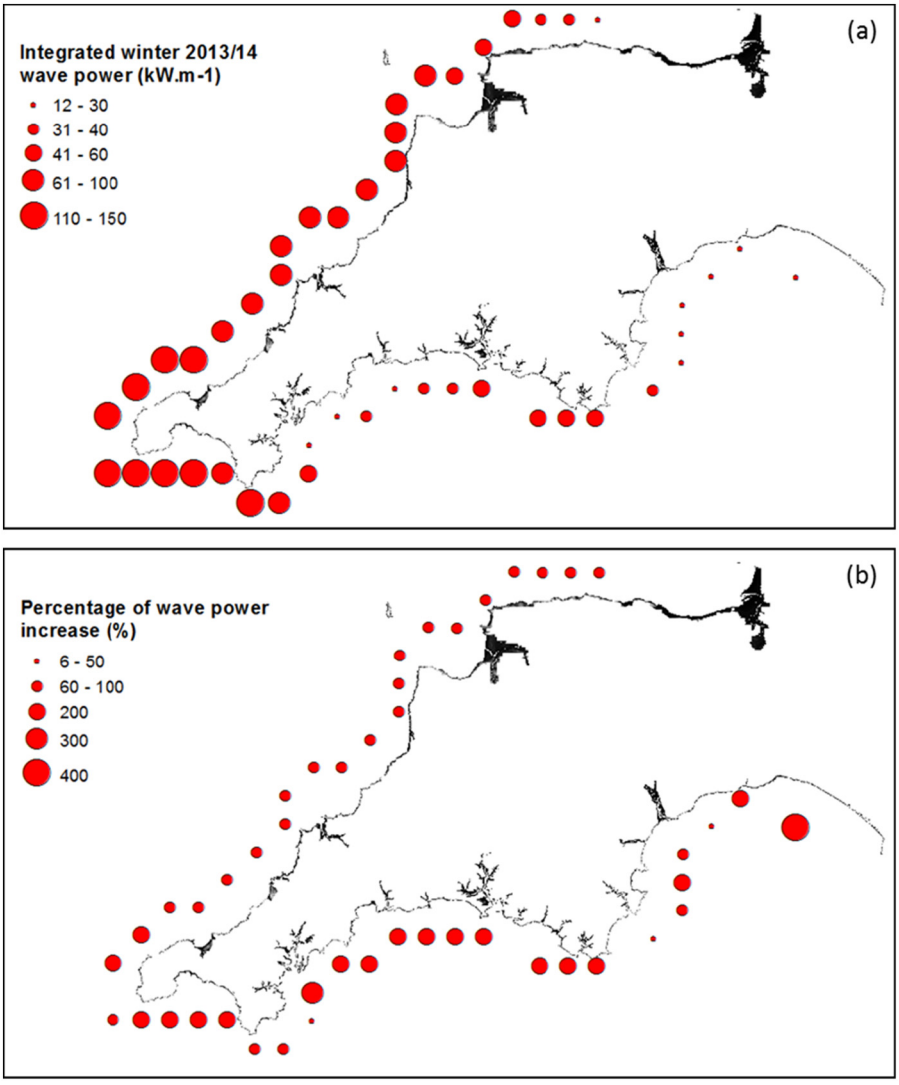

Fig. 5. (a) Along-coast variability in modelled average winter 2013/14 wave power $|P|$ and (b) percentage of wave power increase relative to 2012/13 winter at 46 'deep-water' grid points along the SW coast of England. This figure is available in colour online at https://www.journals.elsevier.com/geomorphology.

on the same wave variables and the same grid points, the percentage change in the average wave power over the 2013/14 winter period compared to that over the previous winter was calculated. The results show that wave power was around 100% higher along the north coast during the 2013/14 winter while it was much more variable on the south coast with values ranging from no change to a 400% increase (Fig. 5b). Thus, whereas the actual wave power during the 2013/14 winter was higher along the north coast, the wave conditions along the south coast were generally more exceptional, i.e., in greater disequilibrium.

The SW coast of England offers a large range of wave exposure due to its specific geomorphology. Although offshore wave conditions are a good indicator of wave forcing at a regional scale, the impact on beaches is strongly dependent on storm wave direction and shoreline orientation (cf. Masselink et al., 2015). The relationship between the deep-water wave angle and shoreline orientation in determining the relative degree of wave exposure/shelter was considered in a semi-quantitative way. Each study site was associated with one of the 46 wave model grid points and the incident wave angle (0° angle correspond to shore-normal waves) between the variable offshore wave direction and the constant shoreline orientation was integrated over the 3-month winter period. Based on this angle, hourly wave power was decomposed into a cross-shore (normal to shoreline) and a longshore (parallel to shoreline) component. The cross-shore and longshore energy fluxes were subsequently integrated over the whole winter period. The objective of the decomposition into cross-shore and longshore wave energy fluxes is to provide an indication of the inshore wave conditions that are affecting the beaches without having to resort to developing a regional-scale wave propagation model (e.g., SWAN). There are issues with the decomposition of the offshore wave flux into cross-shore and longshore components when the wave approach is away from the coast (e.g., westerly waves approaching an east-facing coastline). In that case, the cross-shore energy flux was set to zero. For computing the longshore wave fluxes, absolute values were used for opposing directions.

Time series of the modelled wave conditions around the SW coast of England is also available within the GoogleEarth database from the online article.

4. Results

An initial analysis of the correlations between the different morphological response parameters for all the 157 beaches reveals that the net volumetric change is strongly and significantly correlated with all other volumetric variables (Table 1). Beaches that have experienced significant erosion ($dQ_{net} \ll 0$) also show a large movement of sediment ($dQ_{gross} \gg 0$) and a considerable lowering over their entire area ($dz \ll 0$), and vice versa. These relatively high correlation coefficients also show cross-shore uniformity in terms of response type: when the whole beach erodes ($dQ_{net} < 0$), both upper and lower beach areas are likely to erode as well (dQ_{upper} and $dQ_{lower} < 0$; R = 0.75 and R = 0.88, respectively). However, the quantities of sediment lost or gained in the upper and lower beach area are weakly correlated (R = 0.34). There is no clear relation between the volumetric changes in the coastal dune area (dQ_{dune}) and the other volumetric changes. The alongshore variability in morphological response parameterised by *LVI* shows relatively modest correlation coefficients with the other variables and this index therefore fulfils its intended purpose by complementing, rather than duplicating, the volumetric change parameters.

Table 1
Pearson's correlation coefficients, R, between beach response variables (dQ_{net}: net volumetric change per unit m beach width; dQ_{gross}: gross volumetric change per unit m beach width; dZ: mean vertical elevation change; dQ_{upper}: net volumetric change per unit m beach width over the upper part of the beach; dQ_{lower}: net volumetric change per unit m beach width over the lower part of the beach; dQ_{dune}: net volumetric change per unit m beach width over the dunes; *LVI*: longshore variation index). Correlations exceeding the 99% confidence level are specified using bold text.

	dQ_{net}	dQ_{gross}	dZ	dQ_{upper}	dQ_{lower}	dQ_{dune}	*LVI*
dQ_{net}		**−0.78**	**+0.79**	**+0.75**	**+0.88**	**+0.38**	**+0.46**
dQ_{gross}			**−0.47**	**−0.56**	**−0.70**	**−0.25**	**−0.31**
dZ				**+0.49**	**+0.74**	**+0.43**	**+0.31**
dQ_{upper}					**+0.34**	**+0.47**	**+0.34**
dQ_{lower}						+0.14	**+0.41**
dQ_{dune}							+0.07
LVI							

The along-coast variation in dQ_{net} and *LVI*, and their geographical distribution along the SW coast are presented in Fig. 6. The results show that 104 (66%) beaches lost sediment, while the other 53 (34%) beaches gained sediment during the 2013/14 winter. Large volumes of sediment, of up to 100–200 $m^3 \cdot m^{-1}$, were lost at several study sites, but other sites experienced an increase in the sediment volume of up to 30–60 $m^3 \cdot m^{-1}$ (Fig. 6a). On 59 (38%) beaches, the longshore variation index exceeded 0.7 while for the other 98 (62%) beaches, *LVI* < 0.7 (Fig. 6b). Visual observation of the LiDAR data reveals that for *LVI* > 0.7, the morphological response is characterized by a very significant longshore variability (cf. Fig. 4).

The storm response parameters dQ_{net} and *LVI* also show a distinct geographical demarcation (Fig. 6c and d). Beaches located on the north coast generally experienced more erosion and a relatively along-shore uniform coastal response. South coast beaches, on the other end, generally eroded less, or even accreted, and displayed considerably greater alongshore variability in the coastal response. Masselink et al. (2015) and Scott et al. (2016) also noted this regional variability in storm response and attributed this to the shoreline orientation in relation to the offshore wave direction. The dominant wave direction during the 2013/14 winter storms was from the west; therefore, the west-facing beaches (including WNW- and WSW-facing), dominantly located on the north coast, were fully exposed to the storm waves, causing extensive and largely alongshore-uniform erosion. On beaches not directly facing the Atlantic storm waves, mainly located on the south coast, the storm waves generally approached from large angles providing opportunity for alongshore redistribution of sediment, resulting in both relatively modest sediment losses and large alongshore variability in the coastal response. However, the relation between wave angle and shoreline orientation only accounts for part of the regional variability in storm response along the SW coast of England. This is further explored in the next section.

5. Grouping of the beach responses

5.1. Hierarchical clustering of the beach responses

Cluster analysis is a multivariate statistical technique for identifying structure within a dataset, and has been successfully employed for classifying beach types (Hegge et al., 1996; Travers, 2007; Scott et al., 2011). Here, the technique will be used to classify storm response characteristics.

A critical first step in the analysis is to define the variables used for identifying the clusters. Section 4 showed the suitability of the net volumetric change dQ_{net} and the longshore variation index *LVI* to quantify storm response. The other volumetric variables were all significantly correlated at a 99% confidence level to the net volumetric change (cf., Table 1) and were not included in the cluster analysis to avoid multi-collinearity issues. The second step is the standardisation of the two variables to assign them an equal weight. Dimensionless normal scores (Gower and Ross, 1969) were obtained by subtracting the population mean from the raw scores and then dividing the difference by the population standard deviation. The third step consists of finding a method to assess the similarity between the different study sites across the two variables used in the analysis. Euclidean distance was chosen to measure this similarity, with higher (lower) values representing greater (lesser) dissimilarity. Finally, the hierarchical clustering is made using

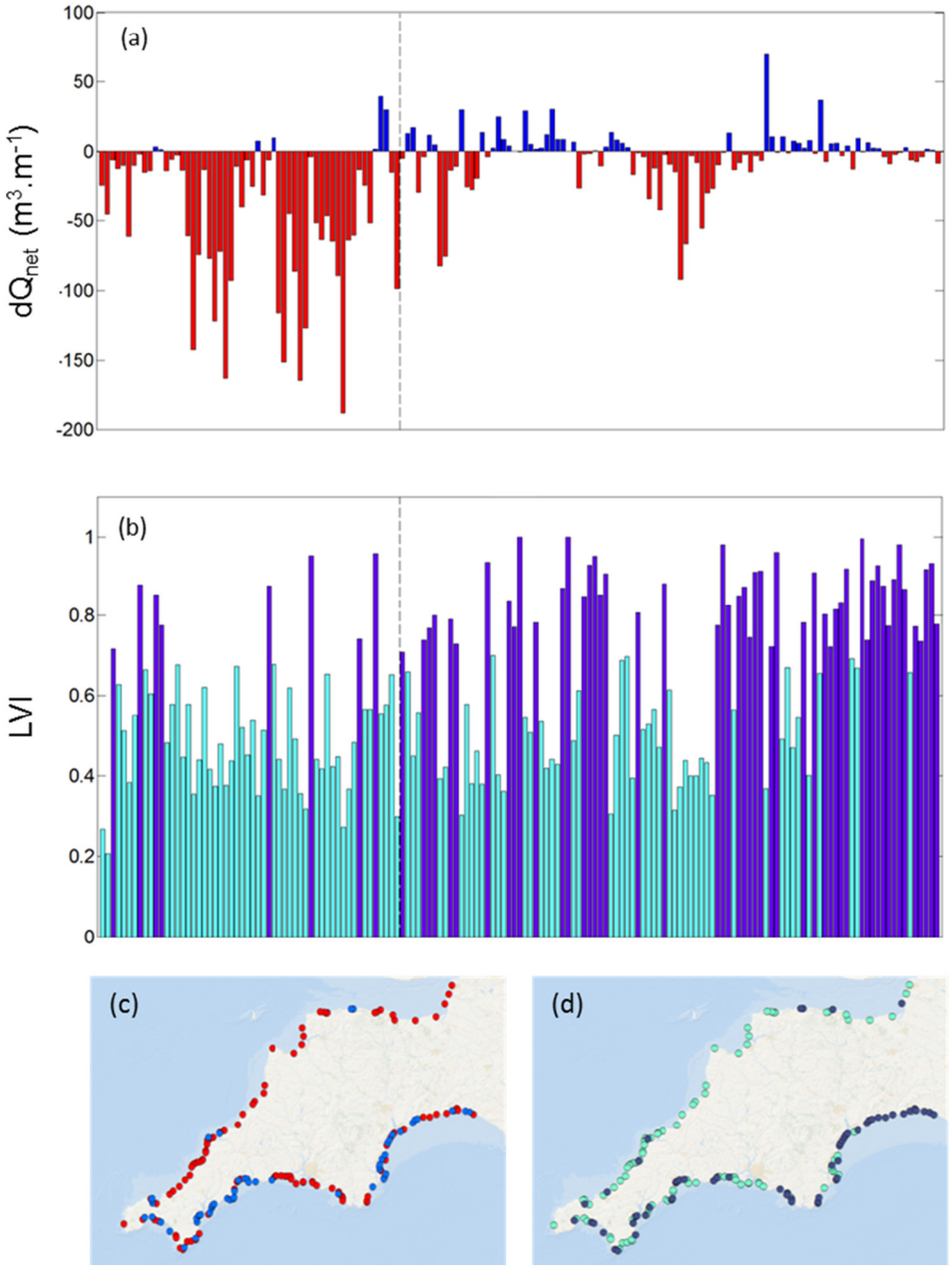

Fig. 6. Along-coast variation in (a) net volumetric change per unit m beach dQ_{net} and (b) longshore variation index *LVI*. Every bar represents a study site and the sites are geographically ordered in an anti-clockwise direction from north to south. The black vertical dashed line marks the separation between the north and the south coast. Geographical distribution of (c) dQ_{net} and (d) *LVI* along the SW coast of England. The colours of the bars and the symbols represent: blue = $dQ_{net} > 0$; red = $dQ_{net} < 0$; clear blue $LVI < 0.7$; purple = $LVI > 0.7$). This figure is available in colour online at https://www.journals.elsevier.com/geomorphology. (For interpretation of the references to colour in this figure legend, the reader is referred to the web version of this article.)

the weighted pair group average method (UPGMA) which defines similarity between clusters as the shortest distance from any object in one cluster to any object in the other (Gower and Ross, 1969). This hierarchical procedure based on an agglomerative algorithm can be represented by a dendrogram (Fig. 7).

Despite the statistical rigour of cluster analysis, there is an element of operator's experience, knowledge and understanding, especially when it comes to finalising the identified clusters and interpreting the results. A cut-off through the dendrogram and its different agglomeration levels were used to decide the final grouping of beaches. This cut-off level was selected based on the knowledge of the different study sites, leading to four different clusters and two outliers (Fig. 7).

5.2. Characterisation of the clusters

Box plots of the dQ_{net} and *LVI* values for the four clusters (Fig. 8) are used in combination with examples of the DoDs (Fig. 9) to help interpret the different storm response types:

- Cluster 1 is characterized by the largest sediment losses (cluster-mean $dQ_{net} = -108\ m^3 \cdot m^{-1}$) and the smallest average longshore variation index ($LVI = 0.37$). Watergate Bay located on the north coast is a good example of a Cluster 1 response, showing a large alongshore-uniform sediment loss across the entire supra- and inter-tidal beach disregarding rip channels (Fig. 9b).

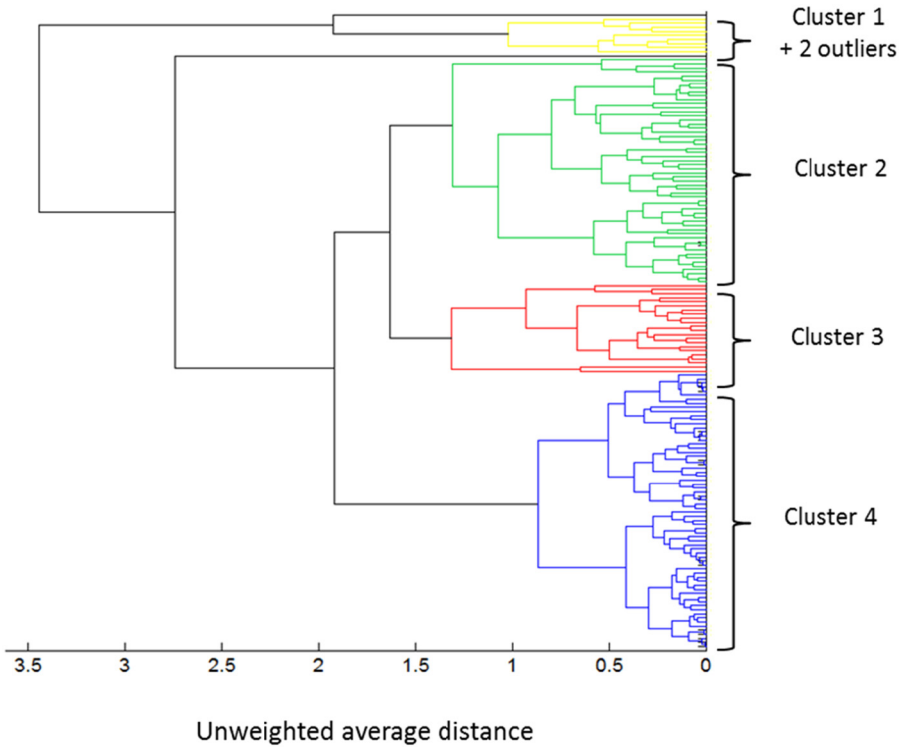

Fig. 7. Dendrogram clustered using weighted pair group average (UPGMA) method showing the hierarchical clustering of the 157 beaches (Cluster 1 = Yellow; Cluster 2 = Green; Cluster 3 = Red; Cluster 4 = Blue). This figure is available in colour online at https://www.journals.elsevier.com/geomorphology. (For interpretation of the references to colour in this figure legend, the reader is referred to the web version of this article.)

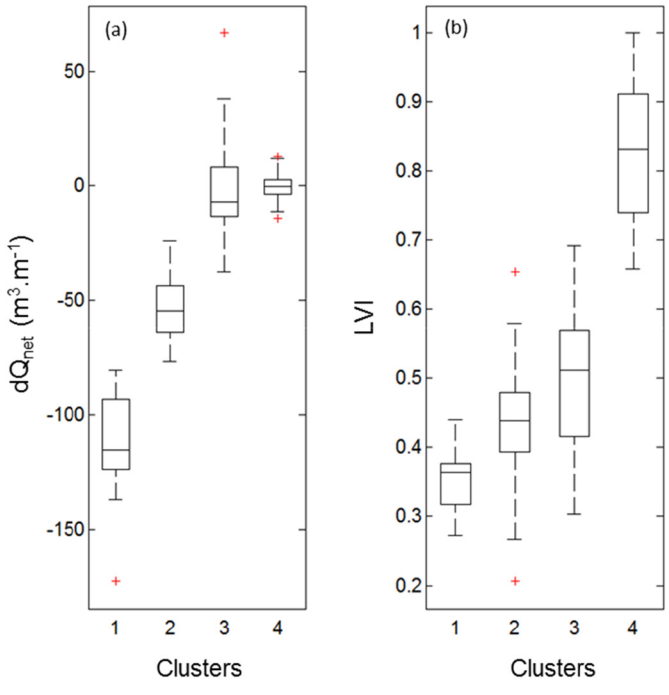

Fig. 8. Box plots showing the distribution of (a) net volumetric change per unit m width dQ_{net} and (b) longshore variation index *LVI* among the four clusters defined by the cluster analysis. Each box plot displays the values of the 25% quantile (bottom line); the median (middle line); the 75% quantile (top line). The maximum whisker length is specified as 1.0 times the interquartile range, and data points beyond the whiskers are displayed using red crosses. This figure is available in colour online at https://www.journals.elsevier.com/geomorphology. (For interpretation of the references to colour in this figure legend, the reader is referred to the web version of this article.)

- Cluster 2 is characterized by considerable sediment losses (cluster-mean $dQ_{net} = -53\ m^3 \cdot m^{-1}$) and limited alongshore-variability in the morphological response ($LVI = 0.44$). This cluster is similar to the previous cluster, but with less extreme sediment losses. A good example of a Cluster 2 response is Croyde located on the north coast, where the deposition across the lower part of the beach profile partly balances the upper beach erosion (Fig. 9a).
- Cluster 3 is characterized by small net changes in the sediment volume (cluster-mean $dQ_{net} = -3\ m^3 \cdot m^{-1}$) and some alongshore variability in the morphological response ($LVI = 0.51$). Broadsands located on the south coast is a good example of a Cluster 3 response, showing limited net morphological changes because deposition (upper and lower beach) and erosion (mid-beach) are more or less balanced (Fig. 9c).
- Cluster 4 is very different from the previous three clusters in that the net volumetric change is very small (cluster-mean $dQ_{net} = -1\ m^3/m$) across all beaches in this cluster, but the alongshore variability in the morphological response is very large ($LVI = 0.83$). A good example of a Cluster 4 response is Praa Sands located on the south coast, where the erosion in the western part of the beach is almost completely balanced by the accretion at the eastern end of the beach (Fig. 9d).

Sediment volumetric change was also considered at different levels on the beach (dQ_{upper} and dQ_{lower}). These response parameters were not included in the cluster analysis, because they did not contribute to a better definition of the clusters, but their consideration can shed additional light on the cross-shore sediment exchange for the different clusters. The values for dQ_{upper} and dQ_{lower} for all 157 beaches are plotted in a scatter diagram that comprises four distinct 'quadrants' (Fig. 10). The top-left and bottom-right quadrants represent a vertically non-uniform morphological response with a pivot point: the beach is either flattening

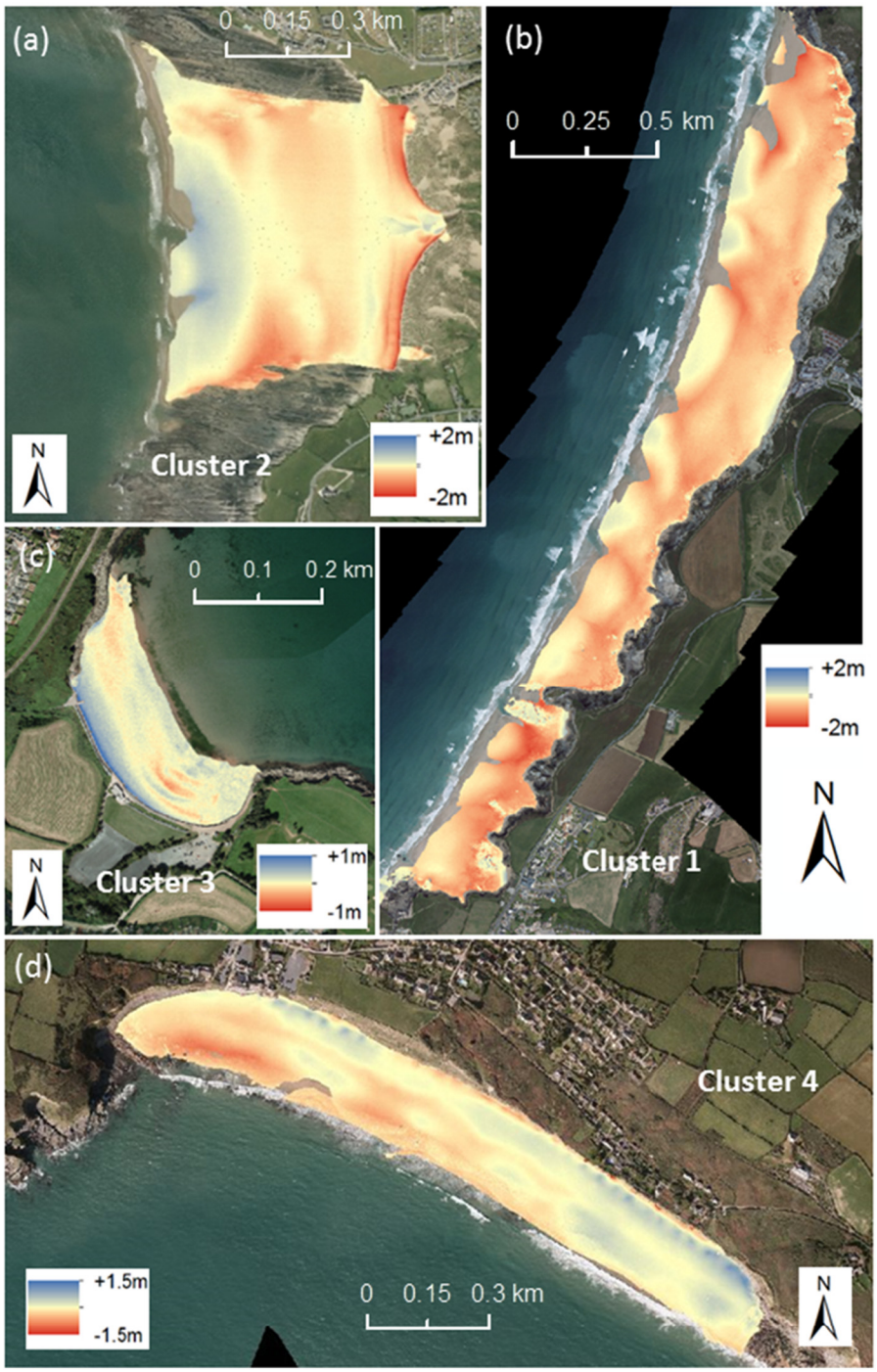

Fig. 9. Examples of DODs obtained from LiDAR data at (a) Croyde beach #17 (Cluster 2 example) surveyed in May 2012 and June 2014; (b) Watergate Bay #39 (Cluster 1 example) surveyed in April 2012 and April 2014; (c) Broadsands #130 (Cluster 3 example) surveyed in April 2012 and April 2014; Praa Sands #62 (Cluster 4 example) surveyed in October 2010 and May 2014. Erosion is coloured in red whereas accretion is coloured in blue. This figure is available in colour online at https://www.journals.elsevier.com/geomorphology. (For interpretation of the references to colour in this figure legend, the reader is referred to the web version of this article.)

(upper beach erosion – lower beach accretion) or steepening (upper beach accretion – lower beach erosion). The top-right and bottom-left quadrants represent a vertically uniform response: the beach either advances or retreats. The vast majority of the beaches in Clusters 1 and 2 eroded and are located in the bottom-left quadrant, indicating that both upper and lower beach areas lost sediment. It is suggested that these beaches mainly lost sediment offshore due to cross-shore sediment transport processes. Beaches in Cluster 3 are located tightly around the origin, but are spread across all four quadrants, suggesting that the full range of cross-shore responses are represented, including vertical rotation due to cross-shore sediment exchange. Beaches in Cluster 4 are concentrated even closer around the origin of the diagram because the dominant sediment exchange occurred in an alongshore direction without large net changes in the sediment volume.

5.3. Role of wave forcing, sand dunes and geology

The cluster analysis is based on the morphological response and does not consider the role of wave forcing or geology. Box plots of three different variables representing wave forcing and geological

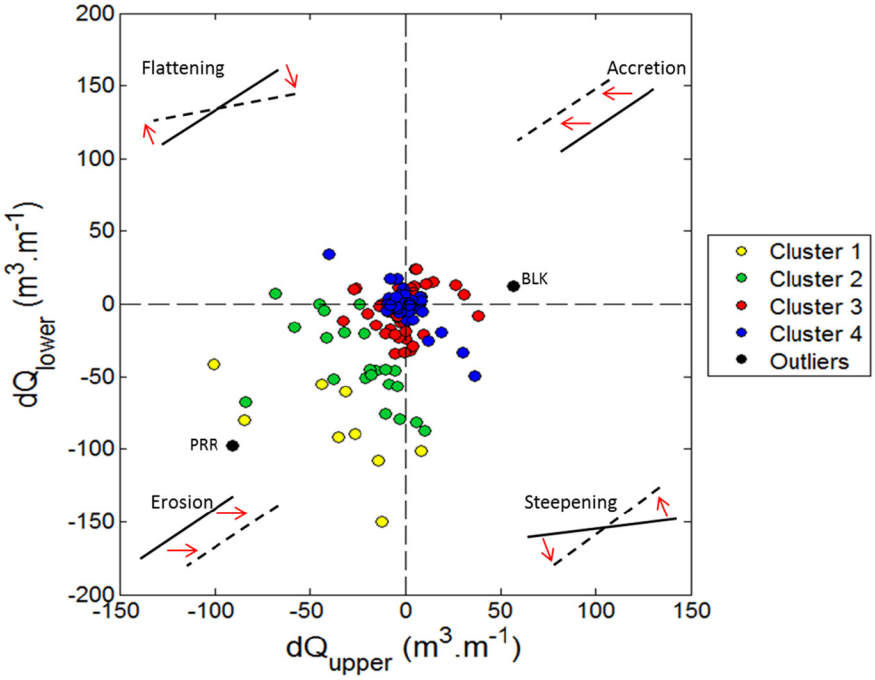

Fig. 10. Scatter plot of dQ_{upper} and dQ_{lower} with the symbol colour representing the cluster type (Cluster 1 = Yellow; Cluster 2 = Green; Cluster 3 = Red; Cluster 4 = Blue; Outliers = Black with PRR = Perran Sands #46 and BLK = Blackpool Sands #125). The diagrams in the corners of the plot are schematic profile responses typical for each of the quadrants, with solid and dashed line representing the profile before and after the 2013/14 winter storms, respectively. This figure is available in colour online at https://www.journals.elsevier.com/geomorphology. (For interpretation of the references to colour in this figure legend, the reader is referred to the web version of this article.)

setting for the four clusters are used to relate these boundary conditions to the different storm response types (Fig.11, top panel).

The parameters used are: incident wave angle (0° angle correspond to shore-normal waves) (Fig. 11a); cross-shore wave power (Fig. 11b); and the normalized beach length *NBL* (Fig. 11c). Cluster 1 is characterized by the smallest incident wave angles (c. 10°) and highest values of cross-shore wave power (c. 170 $kW \cdot m^{-1}$), and these beaches are considered 'fully exposed' to the prevailing storm swell. Cluster 2 shows larger incident wave angles (c. 20°) and relatively more moderate cross-shore power (c. 120 $kW \cdot m^{-1}$), also characterized by a higher standard variation for both parameters. Cluster 2 beaches are considered 'semi-sheltered' in comparison to Cluster 1 beaches. Clusters 3 and 4 are characterized by the largest incident wave angles (60 and 55°, respectively) and the smallest cross-shore wave power (30 and 25 $kW \cdot m^{-1}$, respectively). Beaches classified in these two clusters are thus considered 'sheltered' in comparison to Cluster 1 and 2 beaches.

Cluster 1, 2 and 3 show relatively equivalent mean *NBL* values (4, 3.5 and 3.5, respectively), while Cluster 4 clearly shows higher mean values (8.5) and a larger standard deviation. Cluster 3 and Cluster 4 beaches were therefore separated in two categories: sheltered short and sheltered long beaches, even if some Cluster 4 beaches are also relatively short.

The increase in the wave power during the 2013/14 winter compared to the 2012/13 winter, the longshore wave power and the sediment volume changes over the dunes (dQ_{dunes}) were also parameterised but no clear distinction between the 4 clusters seemed to emerge and were therefore excluded from the analysis.

6. Discussion

The wave conditions experienced during the 2013/14 winter along the Atlantic coast of Europe represent the most energetic since at least 1948 and have had a very significant impact on the coastline of Western Europe (Masselink et al., 2016). A limited data set of the 2013/14 winter storm response on 30 beaches in SW England, based on cross-shore profiles, was discussed by Masselink et al. (2015) and highlighted the predominantly cross-shore profile response on the north coast and longshore response on the south coast. Here, we considerably extend this analysis by using LiDAR data to investigate the full-beach storm response of >150 beaches.

The LiDAR data were used to derive various morphological response variables for each of the beach sites and two of these, the net volumetric change dQ_{net} and the alongshore variability in the beach response *LVI*, were used as the basis for a cluster analysis. Four clusters, each representing distinctive morphological responses during the 2013/4 winter period were identified: (1) fully exposed beaches that experienced large and alongshore uniform sediment losses; (2) semi-exposed beaches that experienced medium alongshore uniform sediment losses; (3) sheltered short beaches that experienced limited alongshore variability in beach response, but insignificant net sediment change; and (4) sheltered long beaches that experienced considerable alongshore variability in beach response, but insignificant net sediment change. However, this classification applies to the beach response to a sequence of Atlantic storms from the southwest quadrant and is unlikely to be representative for the beach response to less frequent storms coming from any of the other directions. The geographical distribution along the coast of SW England of these beach response types and their main characteristics are presented in Fig. 12 and Table 2, respectively.

On a regional scale, this study showed that one of the key factors that discriminates between the different storm responses is the orientation of the beach in relation to the prevailing wave direction, in other words, the degree of exposure to storm waves. This agrees with the findings of Blaise et al. (2015), who investigated beach response along the coastline of Brittany in France during the 2013/14 winter and found that the north and south Brittany coast responded differently to storm waves with varying direction. Furthermore, Castelle et al. (2015) reported dune retreat in excess of 10 m and net volumetric changes >100 $m^3 \cdot m^{-1}$ along the exposed SW coastline of France (Gironde, Landes) and this was similar to the storm response observed along the fully exposed beaches on the north coast of Cornwall. The relatively less-exposed Sefton coast (northwest England) suffered from similar net volumetric changes (c. 40 $m^3 \cdot m^{-1}$; Pye and Blott, 2016),

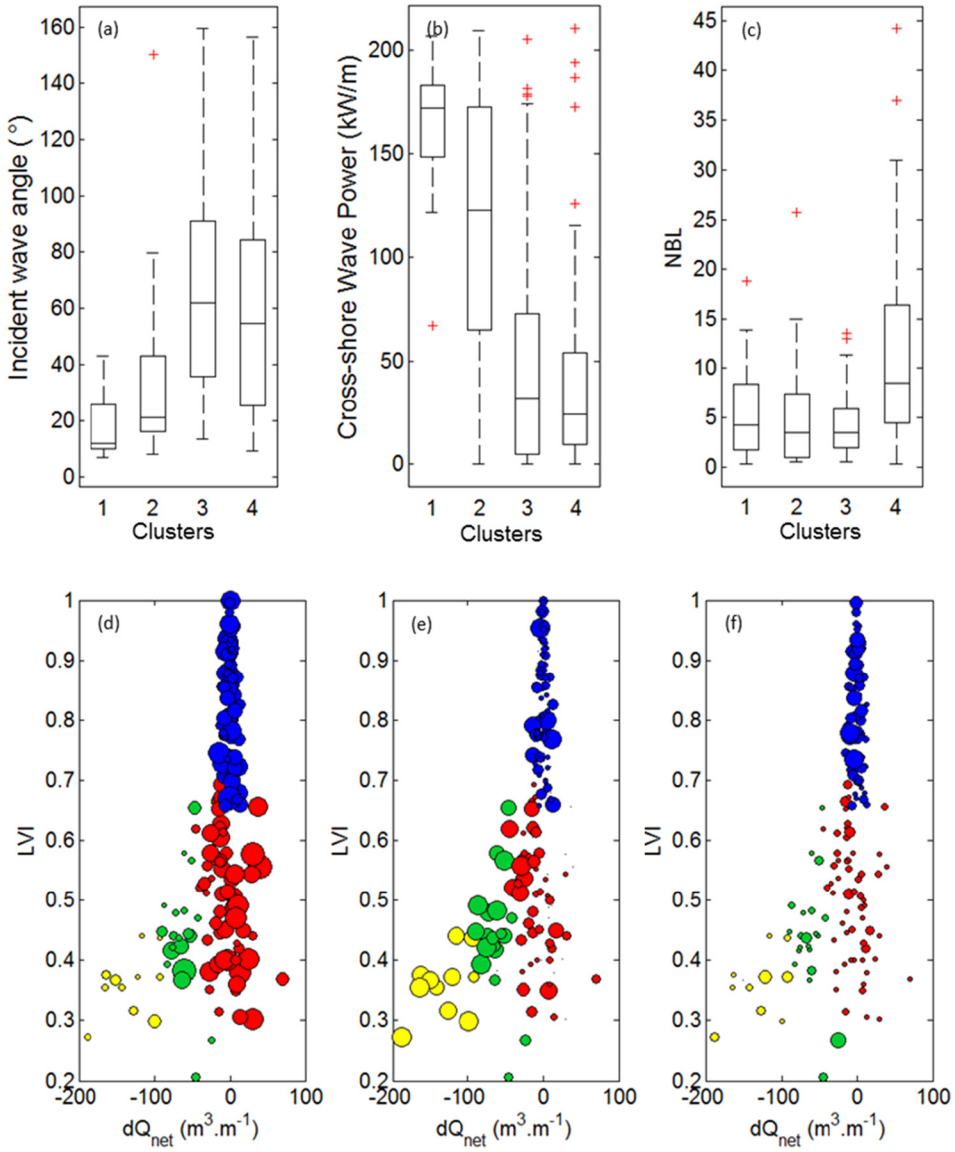

Fig. 11. Top panel: box plots showing the distribution of (a) incident wave angle, (b) cross-shore wave power, (c) normalized beach length among the four clusters defined by the cluster analysis. Each box plot displays the values of the 25% quantile (bottom line); the median (middle line); the 75% quantile (top line). The maximum whisker length is specified as 1.0 times the interquartile range, and data points beyond the whiskers are displayed using red crosses. Bottom panel: scatter plots of net volumetric change dQ_{net} and longshore variation index *LVI* with the symbol colour representing the cluster type (Cluster 1 = Yellow; Cluster 2 = Green; Cluster 3 = Red; Cluster 4 = Blue). The symbols are scaled according the different variables (a) incident wave angle; (b) cross-shore wave power; (c) normalized beach length. This figure is available in colour online at https://www.journals.elsevier.com/geomorphology. (For interpretation of the references to colour in this figure legend, the reader is referred to the web version of this article.)

compare to the semi-exposed beaches presented in our study. Along the south coast of the study area, the prevailing oblique wave approach due to the predominant W-SW storm tracks is very likely to have induced clockwise beach rotation on many of the beaches, similar to that observed at Slapton Sands #124 by Ruiz de Alegria-Arzaburu and Masselink (2010). Such rotational behaviour has also been demonstrated in other studies of large embayed beaches (e.g., Ojeda and Guillen, 2008; Turki et al., 2013; Thomas et al., 2015). A second type of beach rotation, not induced by obliquely-incident waves but by an alongshore gradient in the wave energy level (Harley et al., 2015), was also observed at a few sites on the north coast of Cornwall.

However, the degree of wave exposure was not the only factor in controlling the beach response type to extreme storm activity. Several studies (Jackson et al., 2005; Short, 2010; Loureiro et al., 2012) have argued that the presence of physical boundaries can significantly affect sediment transport and morphodynamics. In the present study, this is particularly highlighted by the difference in storm response between short and long beaches subjected to similar wave exposure along the south coast. Whereas the short beaches experienced limited beach erosion, or even net accretion, and a largely alongshore-uniform response, the long beaches displayed contrasting responses at opposing ends of the embayment.

The geographical distribution of the different types of beach response along the SW coast of England shows regional coherent behaviour: cross-shore sediment transport is dominant on the north coast, whereas beach rotation largely occurs along the south coast. Studies along the East coast of Australia also showed the existence of regionally coherent behaviour among similar beaches exposed to the same regional-scale wave and climate forcing (Short et al., 2014; Bracs et al., 2016). However, this coherence can be disrupted by significant changes in the shoreline orientation and/or local factors (e.g., islands, headlands, rock platforms, river outflows). St. Ives Bay, located on the north coast, exemplifies such a spatial change in beach response (Fig. 13). Here, the bay includes four sandy beaches, separated from each other by headlands and the Hayle River (Fig. 13a), and from north-east to south-west these beaches change in orientation from facing NW to NE. The

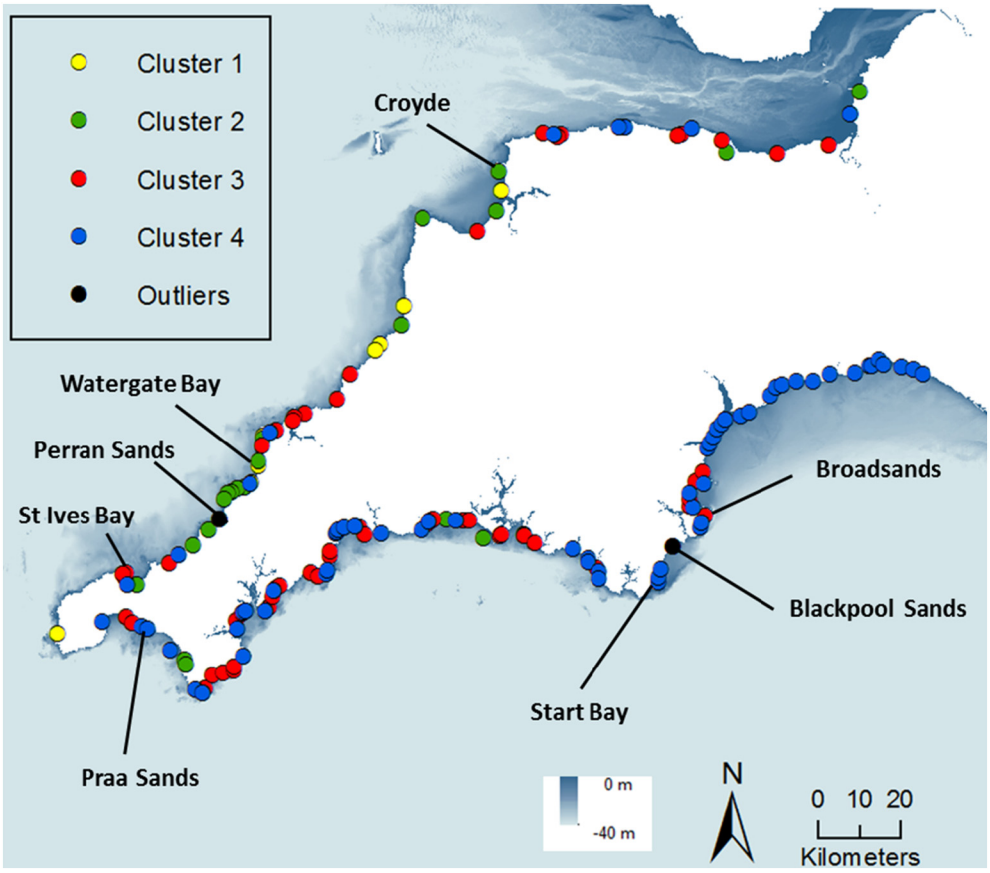

Fig. 12. Geographical distribution of the 157 beaches in the LiDAR dataset and their cluster type (Cluster 1 = Yellow; Cluster 2 = Green; Cluster 3 = Red; Cluster 4 = Blue; Outliers = Black). The four beach examples presented earlier (Fig. 9.) and the two bays presented later (Fig. 13) are also located. This figure is available in colour online at https://www.journals.elsevier.com/geomorphology. (For interpretation of the references to colour in this figure legend, the reader is referred to the web version of this article.)

difference in wave exposure during the 2013/14 winter therefore resulted in neighbouring beaches exhibiting contrasting response types with one Cluster 2 beach (Gwythian #51), two cluster 3 beaches (St Ives #53, Porthgwidden #54) and one cluster 4 beaches (Carbis #52).

The accretion of many of the Cluster 3 beaches during extreme storm conditions also raises the question of the sediment connectivity between adjacent beaches in the same embayment. This is further illustrated by the response of the gravel beaches in Start Bay, located on the south coast (Fig. 13b). Each of these gravel beaches are a separate entity over the most of the tidal cycle and they appear to have behaved independently during the 2013/14 winter with three of the four beaches (Hallsands #122, Beesands #123 and Slapton Sands #124) clearly rotating in response to northward littoral drift. However, the northern-most beach (Blackpool Sands #125) demonstrated very considerable accretion ($dQ_{net} = 66\ m^3 \cdot m^{-1}$) across its entire length and was in fact one of the two outliers in the cluster analysis. The reason for the large increase in sediment volume on Blackpool Sands is that sediment transported northward on Slapton Sands, bypassed the rocky stretch between the two beaches. This process of headland bypassing (Goodwin et al., 2013; Keshtpoor et al., 2013; Mortlock and Goodwin, 2016; Vieira da Silva et al., 2016) is considered important along the embayed SW coast of England and is currently the subject of further investigation.

Several modelling and empirical studies have found an increase in Atlantic storminess over the last few decades (Wang and Swail, 2002; Dodet et al., 2010; Young et al., 2011; Bertin et al., 2013) and this classification of beach response may provide an appropriate framework for considering extreme storm hazards. The classification may also be useful to provide insights into storm recovery. For example, the south embayment of Perran Sands #46, characterized by extensive cross-shore erosion during the 2013/14 winter, has recovered by 50% within 1 year, whereas Slapton Sands #124, which rotated, has not demonstrated any recovery due to the lack of opposing wave direction events (Scott et al., 2016). In 2017, three years after the 2013/14 winter, many exposed and semi-exposed beaches along the southwest coast of England only show partial recovery in comparison to their pre-storm

Table 2
Average values of net volumetric change dQ_{net}, longshore variation index *LVI*, incident wave angle, cross-shore wave power and beach normalized *NBL* for the four beach responses identified: (1) fully exposed beaches; (2) semi-exposed beaches; (3) sheltered short beaches; and (4) sheltered long beaches.

	dQnet ($m^3 \cdot m^{-1}$)	*LVI*	Inc. wave angle (°)	Cross-shore wave power ($kW \cdot m^{-1}$)	*NBL*
Fully exposed beaches	~−100	~0.4	~10	~170	~4
Semi-exposed beaches	~−50	~0.45	~20	~120	~3.5
Sheltered short beaches	~0	~0.5	~60	~30	~3.5
Sheltered long beaches	~0	~0.8	~55	~25	~8.5

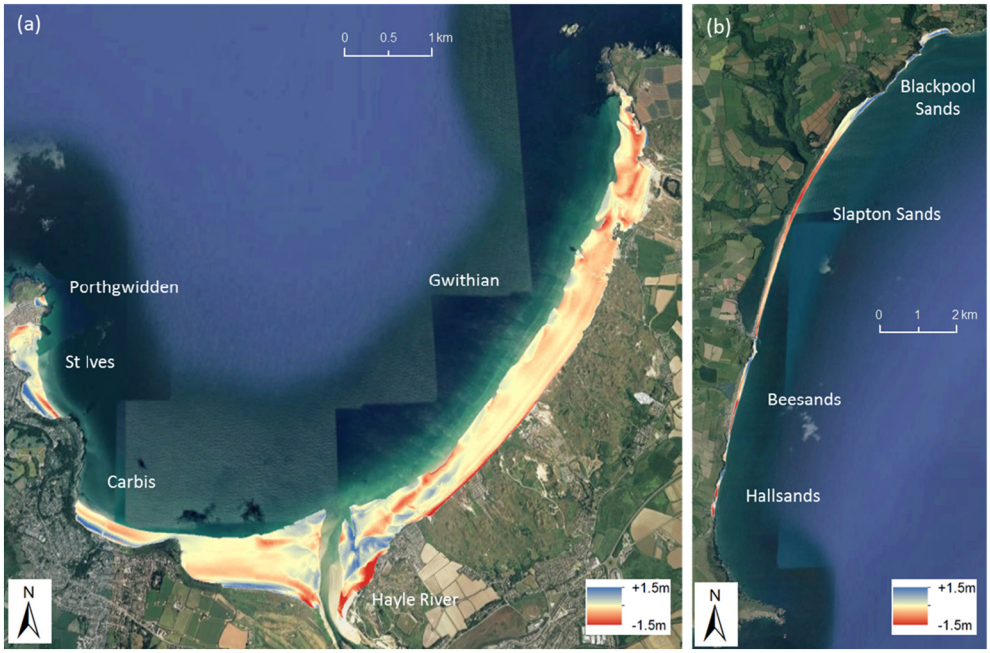

Fig. 13. DoDs obtained from LiDAR data along (a) St. Ives Bay beach surveyed in April 2012 and April 2014, and (b) Start Bay surveyed in April 2012 and April 2014, illustrating spatial change in beach response and sediment connectivity between adjacent beaches at a local scale. Their location along the south west coast of England is presented in Fig. 12. Erosion is coloured in red whereas accretion is coloured in blue. This figure is available in colour online at https://www.journals.elsevier.com/geomorphology. (For interpretation of the references to colour in this figure legend, the reader is referred to the web version of this article.)

state in 2013, whereas most sheltered long beaches have not recovered at all (Burvingt et al., 2017).

7. Conclusions

During the 2013/14 winter, the south west coast of England was subjected to a sequence of large, storm-induced wave events, representing the most energetic period of waves in the last 60 years. A unique dataset of pre- and post-storm airborne LiDAR dataset for 157 beaches along this coastline was analysed.

The beach response to these extreme storms was mainly quantified by two parameters: (1) the net volumetric changes over the entire intertidal beach area dQ_{net} which varied between -170 $m^3 \cdot m^{-1}$ and $+66$ $m^3 \cdot m^{-1}$; and (2) a new parameter, the longshore variation index *LVI*, which quantifies the alongshore variability in beach response, and which varied between 0.2 and 1.

Based on the values of dQ_{net} and *LVI*, a cluster analysis was conducted which resulted in the identification of four different beach response types, largely controlled by wave exposure and normalized beach length: (1) fully exposed beaches; (2) semi-exposed beaches; (3) sheltered short beaches; and (4) sheltered long beaches.

The geographical distribution among the four different beach responses to extreme storms showed some regional coherence in behaviour. However, several examples demonstrate that this coherence can be disrupted at a local scale, highlighting the connectivity between beach systems via physical processes like sediment redistribution or/and headland by-passing.

Acknowledgments

This research was funded by NERC grants NE/M004996/1 (Urgency Grant) and NE/N015525/1 (Strategic Highlights Topic grant). The UK Met Office (Dr. Andy Saulter) and Channel Coast Observatory (Emerald Siggory) kindly provided supporting modelled wave data and the LiDAR data, respectively. We also would like to thank Daniel Conley for putting together the GoogleEarth database.

Appendix A. Supplementary data

Supplementary data associated with this article can be found in the online version, at http://dx.doi.org/10.1016/j.geomorph.2017.07.022. These data include the Google map of the most important areas described in this article.

References

Aagaard, T., Hughes, M., Baldock, T., Greenwood, B., Kroon, A., Power, H., 2012. Sediment transport processes and morphodynamics on a reflective beach under storm and non-storm conditions. Mar. Geol. 326-328:154–165. http://dx.doi.org/10.1016/j.margeo.2012.09.004.

Almeida, L.P., Vousdoukas, M.V., Ferreira, O., Rodrigues, B.A., Matias, A., 2012. Thresholds for storm impacts on an exposed sandy coastal area in southern Portugal. Geomorphology 143-144:3–12. http://dx.doi.org/10.1016/j.geomorph.2011.04.047.

Anthony, E.J., 2013. Storms, shoreface morphodynamics, sand supply, and the accretion and erosion of coastal dune barriers in the southern North Sea. Geomorphology 199:8–21. http://dx.doi.org/10.1016/j.geomorph.2012.06.007.

Autret, R., Dodet, G., Fichaut, B., Suanez, S., David, L., Leckler, F., Ardhuin, F., Ammann, J., Grandjean, P., Lallemand, P., Philipot, J.F., 2016. A comprehensive hydro-geomorphic study of cliff-top storm deposits on Banneg Island during winter 2013–2014. Mar. Geol. 382, 37–55.

Barnard, P.L., Short, A.D., Harley, M.D., Splinter, K.D., Vitousek, S., Turner, I.L., Allan, J., Banno, M., Bryan, K.R., Doria, A., Hansen, J.E., Kato, S., Kuriyama, Y., Randall-Goodwin, E., Ruggiero, P., Walker, I.J., Heathfield, D.K., 2015. Coastal vulnerability across the Pacific dominated by El Nino/Southern Oscillation. Nat. Geosci. 8: 801–808. http://dx.doi.org/10.1038/NGEO2539.

Bertin, X., Prouteau, E., Letetrel, C., 2013. A significant increase in wave height in the North Atlantic Ocean over the 20th century. Glob. Planet. Chang. 106:77–83. http://dx.doi.org/10.1016/j.gloplacha.2013.03.009.

Blaise, E., Suanez, S., Stéphan, P., Fichaut, B., David, L., Cuq, V., Autret, R., Houron, J., Rouan, M., Floc'h, F., Ardhuin, F., Cancouët, R., Davidson, R., Costa, S., Delacourt, C., 2015. Bilan des tempêtes de l'hiver 2013–2014 sur la dynamique du recul du trait de côte en Bretagne. Geomorphol. Relief Processus Environ. 21:267–292. http://dx.doi.org/10.4000/geomorphologie.11104.

Bracs, M.A., Turner, I.L., Splinter, K.D., Short, A.D., Mortlock, T.R., 2016. Synchronised patterns of erosion and deposition observed at two beaches. Mar. Geol. 380:196–204. http://dx.doi.org/10.1016/j.margeo.2016.04.016.

Bromirski, P.D., Cayan, D.R., 2015. Wave power variability and trends across the North Atlantic influenced by decadal climate patterns. J. Geophys. Res. Oceans 120: 3419–3443. http://dx.doi.org/10.1002/2014JC010440.

Burvingt, O., Masselink, G., Russell, P., Scott, T., 2017. Beach evolution and recovery from a sequence of extreme storms. Coastal Dynamics 2017 Proceedings 1199–1210.

Castelle, B., Coco, G., 2012. The morphodynamics of rip channels on embayed beaches. Cont. Shelf Res. 43:10–23. http://dx.doi.org/10.1016/j.csr.2012.04.010.
Castelle, B., Marieu, V., Bujan, S., Ferreira, S., Parisot, J.P., Capo, S., Senechal, N., Chouzenoux, T., 2014. Equilibrium shoreline modelling of a high-energy meso-macrotidal multiple-barred beach. Mar. Geol. 347, 85–94.
Castelle, B., Marieu, V., Bujan, S., Splinter, K.D., Robinet, A., Sénéchal, N., Ferreira, S., 2015. Impact of the winter 2013–2014 series of severe Western Europe storms on a double-barred sandy coast: beach and dune erosion and megacusp embayments. Geomorphology 238:135–148. http://dx.doi.org/10.1016/j.geomorph.2015.03.006.
Castelle, B., Dodet, G., Masselink, G., Scott, T., 2017. A new climate index controlling winter wave activity along the Atlantic coast of Europe: the West Europe Pressure Anomaly. Geophys. Res. Lett. 44. http://dx.doi.org/10.1002/2016GL072379.
Clayton, K., Shamoon, N., 1998. New approach to the relief of Great Britain II. A classification of rocks based on relative resistance to denudation. Geomorphology 25, 155–171.
Coco, G., Senechal, N., Rejas, A., Bryan, K.R., Capo, S., Parisot, J.P., Brown, J.A., MacMahan, J.H.M., 2014. Beach response to a sequence of extreme storms. Geomorphology 204:493–501. http://dx.doi.org/10.1016/j.geomorph.2013.08.028.
Cooper, J.A.G., Jackson, D.W.T., Navas, F., McKenna, J., Malvarez, G., 2004. Identifying storm impacts on an embayed, high-energy coastline: examples from western Ireland. Mar. Geol. 210:261–280. http://dx.doi.org/10.1016/j.margeo.2004.05.012.
Costas, S., Alejo, I., Vila-Concejo, A., Nombela, M.A., 2005. Persistence of storm-induced morphology on a modal low-energy beach: a case study from NW-Iberian Peninsula. Mar. Geol. 224:43–56. http://dx.doi.org/10.1016/j.margeo.2005.08.003.
Davidson, M.A., Splinter, K.D., Turner, I.L., 2013. A simple equilibrium model for predicting shoreline change. Coast. Eng. 73:191–202. http://dx.doi.org/10.1016/j.coastaleng.2012.11.002.
Department for Business, Enterprise and Regulatory Reform (BERR), 2008. Atlas of UK Marine Renewable Energy Resources. Technical Report. ABP Marine Environmental Research Ltd. (R/3719/8 R.1432).
Dissanayake, P., Brown, J., Wisse, P., Karunarathna, H., 2015. Effects of storm clustering on beach/dune evolution. Mar. Geol. 370:63–75. http://dx.doi.org/10.1016/j.margeo.2015.10.010.
Dodet, G., Bertin, X., Taborda, R., 2010. Wave climate variability in the North-East Atlantic Ocean over the last six decades. Ocean Model 31:120–131. http://dx.doi.org/10.1016/j.ocemod.2009.10.010.
Goodwin, I.D., Freeman, R., Blackmore, K., 2013. An insight into headland sand bypassing and wave climate variability from shoreface bathymetric change at Byron Bay, New South Wales, Australia. Mar. Geol. 341:29–45. http://dx.doi.org/10.1016/j.margeo.2013.05.005.
Gower, J.C., Ross, G.J.S., 1969. Minimum spanning trees and single linkage cluster analysis. J. R. Soc. (Appl. Stat.) 18:54–64. http://dx.doi.org/10.2307/2346439.
Haerens, P., Bolle, A., Trouw, K., Houthuys, R., 2012. Definition of storm thresholds for significant morphological change of the sandy beaches along the Belgian coastline. Geomorphology 143-144:104–117. http://dx.doi.org/10.1016/j.geomorph.2011.09.015.
Harley, M., Turner, I., Short, A., Ranasinghe, R., 2011. A re-evaluation of coastal embayment rotation: the dominance of cross-shore versus alongshore sediment transport processes, Collaroy-Narrabeen Beach, SE Australia. J. Geophys. Res. Earth 116, F04033. http://dx.doi.org/10.1029/2011JF001989.
Harley, M.D., Turner, I.L., Short, A.D., 2015. New insights into embayed beach rotation: the importance of wave exposure and cross-shore processes. J. Geophys. Res. Earth 120: 1470–1484. http://dx.doi.org/10.1002/2014JF003390.
Hegge, B., Eliot, I., Hsu, J., 1996. Sheltered sandy beaches of Southwestern Australia. J. Coast. Res. 12 (3), 748.
Herbich, J.B., 2000. Handbook of Coastal Engineering. McGraw-Hill Professional, New York City, USA.
Jackson, D.W.T., Cooper, J.A.G., del Rio, L., 2005. Geological control of beach morphodynamic state. Mar. Geol. 216:297–314. http://dx.doi.org/10.1016/j.margeo.2005.02.021.
Jackson, N.L., Nordstrom, K.F., Feagin, R.A., Smith, W.K., 2013. Coastal geomorphology and restoration. Geomorphology 199:1–7. http://dx.doi.org/10.1016/j.geomorph.2013.06.027.
Karunarathna, H., Pender, D., Ranasinghe, R., Short, A.D., Reeve, D.E., 2014. The effects of storm clustering on beach profile variability. Mar. Geol. 348:103–112. http://dx.doi.org/10.1016/j.margeo.2013.12.007.
Keshtpoor, M., Puelo, J.A., Gebert, J., Plant, N.G., 2013. Beach response to a fixed sand bypassing system. Coast. Eng. 73:28–42. http://dx.doi.org/10.1016/j.coastaleng.2012.09.006.
Kidson, C., Gilbertson, D., Haynes, J., Heywort, A., Hughes, C., Whatley, R., 2008. Interglacial marine deposits of the Somerset level, south west England. Boreas 7 (4):215–228. http://dx.doi.org/10.1111/j.1502-3885.1978.tb00280.x.
Lee, G., Nicholls, R.J., Birkemeier, W.A., 1998. Storm-driven variability of the beach-nearshore profile at Duck, North Carolina, USA, 1981–1991. Mar. Geol. 148, 163–177.
Loureiro, C., Ferreira, O., Cooper, J.A.G., 2012. Geologically constrained morphological variability and boundary effects on embayed beaches. Mar. Geol. 329–331:1–15. http://dx.doi.org/10.1016/j.margeo.2012.09.010.
Lozano, I., Devoy, R.J.N., May, W., Andersen, U., 2004. Storminess and vulnerability along the Atlantic coastlines of Europe: analysis of storm records and of a greenhouse gases induced climate scenario. Mar. Geol. 210:205–225. http://dx.doi.org/10.1016/j.margeo.2004.05.026.
Masselink, G., Scott, T., Davidson, M., Russell, P., Conley, D., 2015. The extreme 2013/2014 winter storms: hydrodynamic forcing and coastal response along the southwest coast of England. Earth Surf. Process. Landf. 41:378–391. http://dx.doi.org/10.1002/esp.3836.
Masselink, G., Castelle, B., Scott, T., Dodet, G., Suanez, S., Jackson, D., Floc'h, F., 2016. Extreme wave activity during 2013/2014 winter and morphological impacts along the Atlantic coast of Europe. Geophys. Res. Lett. 43:2135–2143. http://dx.doi.org/10.1002/2015GL067492.
Moon, I.J., Ginis, I., Hara, T., Tolman, H.L., Wright, C.W., Walsh, E.J., 2003. Numerical simulation of sea surface directional wave spectra under hurricane wind forcing. J. Phys. Oceanogr. 33:1680–1705. http://dx.doi.org/10.1175/2410.1.
Mortlock, T.R., Goodwin, I.D., 2016. Impacts of enhanced central Pacific ENSO on wave climate and headland-bay beach morphology. Cont. Shelf Res. 120:14–25. http://dx.doi.org/10.1016/j.csr.2016.03.007.
Ojeda, E., Guillen, J., 2008. Shoreline dynamics and beach rotation of artificial embayed beaches. Mar. Geol. 253:51–62. http://dx.doi.org/10.1016/j.margeo.2008.03.010.
Prodger, S., Russell, P., Davidson, M., Miles, J., Scott, T., 2016. Understanding and predicting the temporal variability in sediment grain size characteristics on high energy beaches. Mar. Geol. 376:109–117. http://dx.doi.org/10.1016/j.margeo.2016.04.003.
Pye, K., Blott, S.J., 2016. Assessment of beach and dune erosion and accretion using LiDAR: impact of the stormy 2013–14 winter and longer term trends on the Sefton coast, UK. Geomorphology 266:146–167. http://dx.doi.org/10.1016/j.geomorph.2016.05.011.
Qi, H., Cai, F., Lei, G., Cao, H., Shi, F., 2010. The response of three main beach types to tropical storms in South China. Mar. Geol. 275:244–254. http://dx.doi.org/10.1016/j.margeo.2010.06.005.
Ruiz de Alegria-Arzaburu, A., Masselink, G., 2010. Storm response and beach rotation on a gravel beach, Slapton Sands, U.K. Mar. Geol. 278:77–99. http://dx.doi.org/10.1016/j.margeo.2010.09.004.
Sallenger, A.H.J., Krabill, W., Swift, R., Brock, J., 2001. Quantifying hurricane-induced coastal changes using topographic lidar. Coastal Dynamics '01 Proceedings. American Society of Civil Engineers, Reston, Virginia, USA:pp. 1007–1016 http://dx.doi.org/10.1061/40566(260)103.
Saye, S.E., van der Wal, D., Pye, K., Blott, S.J., 2005. Beach-dune morphological relationships and erosion/accretion: an investigation at five sites in England and Wales using LiDAR data. Geomorphology 72:128–155. http://dx.doi.org/10.1016/j.geomorph.2005.05.007.
Scott, T.M., 2009. Beach Morphodynamics and Associated Hazards in the UK. (Ph.D. thesis). University of Plymouth.
Scott, T., Masselink, G., Russell, P., 2011. Morphodynamic characteristics and classification of beaches in England and Wales. Mar. Geol. 286:1–20. http://dx.doi.org/10.1016/j.margeo.2011.04.004.
Scott, T., Masselink, G., O'Hare, T., Saulter, A., Poate, T., Russell, P., Davidson, M., Conley, D., 2016. The extreme 2013/2014 winter storms: beach recovery along the southwest coast of England. Mar. Geol. 382:224–241. http://dx.doi.org/10.1016/j.margeo.2016.10.011.
Senechal, N., Coco, G., Castelle, B., Marieu, V., 2015. Storm impact on the seasonal shoreline dynamics of a meso- to macrotidal open sandy beach (Biscarrosse, France). Geomorphology 228:448–461. http://dx.doi.org/10.1016/j.geomorph.2014.09.025.
Sherman, D.J., Hales, B.U., Potts, M.K., Ellis, J.T., Liu, H., Houser, C., 2013. Impacts of Hurricane Ike on the beaches of the Bolivar Peninsula, TX, USA. Geomorphology 199: 62–81. http://dx.doi.org/10.1016/j.geomorph.2013.06.011.
Short, A.D., 1999. Handbook of Beach and Shoreface Morphodynamics. John Wiley & Sons, Chichester, UK.
Short, A.D., 2010. Role of geological inheritance in Australian beach morphodynamics. Coast. Eng. 57:92–97. http://dx.doi.org/10.1016/j.coastaleng.2009.09.005.
Short, A.D., Bracs, M.A., Turner, I.A., 2014. Beach oscillation and rotation: local and regional response at three beaches in southeast Australia. J. Coast. Res. 66:712–717. http://dx.doi.org/10.2112/SI-120.1.
Splinter, K.D., Carley, J.T., Golshani, A., Tomlinson, R., 2014a. A relationship to describe the cumulative impact of storm clusters on beach erosion. Coast. Eng. 83:49–55. http://dx.doi.org/10.1016/j.coastaleng.2013.10.001.
Splinter, K.D., Turner, I.L., Davidson, M.A., Barnard, P., Castelle, B., Oltman-Shay, J., 2014b. A generalized equilibrium model for predicting daily to interannual shoreline response. J. Geophys. Res. Earth 119 (9):1936–1958. http://dx.doi.org/10.1002/2014JF003106.
Thomas, T., Phillips, M.R., Lock, G., 2015. An analysis of subaerial beach rotation and influences of environmental forcing adjacent to the proposed Swansea Bay tidal lagoon. Appl. Geogr. 62:276–293. http://dx.doi.org/10.1016/j.apgeog.2015.05.005.
Travers, A., 2007. Low-energy beach morphology with respect to physical setting: a case study from Cockburn Sound, Southwestern Australia. J. Coast. Res. 23 (2):429–444. http://dx.doi.org/10.2112/04-0275.1.
Turki, I., Medina, R., Coco, G., Gonzalez, M., 2013. An equilibrium model to predict shoreline rotation of pocket beaches. Mar. Geol. 346:220–232. http://dx.doi.org/10.1016/j.margeo.2013.08.002.
Vieira da Silva, G., Toldo Jr., E.E., da F. Klein, A.H., Short, A.D., Woodroffe, C.D., 2016. Headland sand bypassing - quantification of net sediment transport in embayed beaches, Santa Catarina Island North Shore, Southern Brazil. Mar. Geol. 379:13–27. http://dx.doi.org/10.1016/j.margeo.2016.05.008.
Wang, X.L., Swail, V.R., 2002. Trends of Atlantic wave extremes as simulated in a 40-yr wave hindcast using kinematically reanalysed wind fields. J. Clim. 15:1020–1035. http://dx.doi.org/10.1175/1520-0442(2002)015<1020:TOAWEA>2.0.CO;2.
Wheaton, J.M., Brasington, J., Darby, S.E., Sear, D.A., 2010. Accounting for uncertainty in DEMs from repeat topographic surveys: improved sediment budgets. Earth Surf. Process. Landf. 35:136–156. http://dx.doi.org/10.1002/esp.1886.
White, S.A., Wang, Y., 2003. Utilizing DEMs derived from LiDAR data to analyze morphologic change in the North Carolina coastline. Remote Sens. Environ. 85:39–47. http://dx.doi.org/10.1016/S0034-4257(02)00185-2.
Young, I.R., Sieger, S., Babanin, A.V., 2011. Global trends in wind speed and wave height. Science 332:451–455. http://dx.doi.org/10.1126/science.1201686.